

# Extreme sensitivity of the spin-splitting and 0.7 anomaly to confining potential in one-dimensional nanoelectronic devices

A. M. Burke,<sup>\*,†</sup> O. Klochan,<sup>†</sup> I. Farrer,<sup>‡</sup> D.A. Ritchie,<sup>‡</sup> A. R. Hamilton,<sup>†</sup> and A. P. Micolich<sup>\*,†</sup>

*School of Physics, University of New South Wales, Sydney NSW 2052, Australia, and Cavendish Laboratory, University of Cambridge, CB3 0HE, U.K.*

E-mail: amburke@unsw.edu.au; adam.micolich@nanoelectronics.physics.unsw.edu.au

## Abstract

Quantum point contacts (QPCs) have shown promise as nanoscale spin-selective components for spintronic applications and are of fundamental interest in the study of electron many-body effects such as the  $0.7 \times 2e^2/h$  anomaly. We report on the dependence of the 1D Landé  $g$ -factor  $g^*$  and 0.7 anomaly on electron density and confinement in QPCs with two different top-gate architectures. We obtain  $g^*$  values up to 2.8 for the lowest 1D subband, significantly exceeding previous in-plane  $g$ -factor values in AlGaAs/GaAs QPCs, and approaching that in InGaAs/InP QPCs. We show that  $g^*$  is highly sensitive to confinement potential, particularly for the lowest 1D subband. This suggests careful management of the QPC's confinement potential may enable the high  $g^*$  desirable for spintronic applications without resorting to narrow-gap materials such as InAs or InSb. The 0.7 anomaly and zero-bias peak are also

---

<sup>\*</sup>To whom correspondence should be addressed

<sup>†</sup>School of Physics, University of New South Wales, Sydney NSW 2052, Australia

<sup>‡</sup>Cavendish Laboratory, University of Cambridge, CB3 0HE, U.K.

highly sensitive to confining potential, explaining the conflicting density dependencies of the 0.7 anomaly in the literature.

**Keywords:** one-dimensional system,  $g$ -factor, quantum point contact, nanoelectronics.

A current focus in nanoelectronics is the development of spintronic devices where spin is used instead of charge for storage, transfer and processing of information.<sup>1</sup> Non-magnetic spintronic device elements are highly desirable;<sup>2</sup> quantum point contacts (QPCs) have shown great promise being used both as individual spin injectors and detectors,<sup>3–5</sup> and in larger device structures for studying phenomena such as spin relaxation<sup>6</sup> and ballistic spin resonance.<sup>7</sup> The QPC is the quintessential one-dimensional (1D) electron system, consisting of a narrow quasi-1D aperture separating two regions of two-dimensional electron gas (2DEG) in a III-V semiconductor heterostructure. It is typically defined electrostatically by applying a negative bias to nanoscale metal gates on the heterostructure surface; its hallmark is a quantized electrical conductance  $G = mG_0$ , where  $G_0 = 2e^2/h$ ,  $e$  is the electron charge,  $h$  is Planck's constant, and  $m$  is the number of spin degenerate 1D subbands beneath the Fermi energy  $E_F$  of the adjacent 2DEG reservoirs.<sup>8,9</sup> The spin properties of QPCs are also of fundamental interest; one example is the conductance anomaly at  $G \sim 0.7G_0$ ,<sup>10</sup> where the interplay between 1D confinement, quasi-bound state formation and exchange-driven spin polarization are not yet fully understood.<sup>11</sup> The combined influence of exchange and 1D confinement are also vital to remarkable behaviors such as spin-charge separation<sup>12</sup> and the formation of electron liquid/solid states in 1D electron systems.<sup>13,14</sup>

An important quantity in considering the spin-properties of QPCs is the effective Landé  $g$ -factor  $g^*$ , the constant of proportionality between the Zeeman splitting of the 1D subbands and the applied magnetic field. The  $g$ -factor  $g_m^*$  for each 1D subband  $m$  is easily measured in QPCs.<sup>15</sup> For spin injection and detection, it is highly desirable to maximize the lowest 1D subband  $g$ -factor  $g_1^*$ , which sets the minimum field required to resolve the spin. The  $g$ -factor is also a useful experimental probe of the exchange interaction.<sup>16</sup> The foundational work on the  $0.7 \times 2e^2/h$  anomaly showed that  $g_m^*$  increases from the bulk GaAs value of 0.44 at  $m = 25$  to  $\sim 1.15$  at  $m < 4$ .<sup>10</sup> This 'exchange-enhancement' effect,<sup>17</sup> also observed in InGaAs/InP QPCs,<sup>18,19</sup> is central to the suggestion that

the 0.7 anomaly is caused by exchange-driven spontaneous spin-polarization within the QPC.<sup>10,17</sup> Remarkably, after 15 years of study of the 0.7 anomaly, little more is known about the dependence of  $g_m^*$  on QPC confinement potential or the electron density  $n$  of the 2DEG in which the QPC is formed.<sup>11</sup>

Here we study how  $g_m^*$  evolves with  $n$  for three samples featuring two different gate architectures for enacting changes in density. We pay particular attention to  $g_1^*$  given its importance for spintronics and the 0.7 anomaly. We obtain  $g_1^*$  values as high as 2.8. This exceeds previous reports for the in-plane  $g$ -factor in GaAs QPCs,<sup>6,10,15,20,21</sup> and approaches both the perpendicular  $g$ -factor recently demonstrated in GaAs QPCs<sup>22</sup> and the lower-bound in-plane  $g^*$  for InGaAs QPCs.<sup>18,19,23</sup> The link between  $g_m^*$  and density is not direct; for example, we see *opposite* trends in  $g_1^*$  with  $n$  for the two architectures. We find that the  $g$ -factor  $g_m^*$ , and  $g_1^*$  in particular, is sensitive to the top-gate configuration. This has important consequences for spintronic applications of QPCs; if high  $g_1^*$  can be obtained in GaAs QPCs by careful management of the QPC's electrostatic potential, it lessens the need to use narrow band-gap materials (e.g., InGaAs, InSb) for which device fabrication is more difficult. The second key result of our work arises from comparing the density dependence of the 0.7 anomaly in the three samples with that of  $g_1^*$  and the lowest 1D subband spacing  $\Delta E_{1,2}$ , a measure of the strength of the 1D confinement. The behavior of the 0.7 anomaly in our devices is consistent with the density dependent spin-gap model<sup>24,25</sup> if the spin-splitting rate is assumed directly proportional to  $\Delta E_{1,2}$ . This highlights the important role that confinement potential plays in the 0.7 anomaly, and provides an explanation for the conflicting reports regarding the density dependence of the 0.7 anomaly in earlier literature.<sup>17,24–32</sup>

We used two different device architectures in this experiment (see Fig. 1a/b), each fabricated on the same heterostructure and featuring a pair of QPC gates (orange) biased at  $V_g$  to define a 1D channel, and a top-gate (yellow) biased at  $V_t$  to independently vary  $n$ . The two devices differ in the location of the top-gate, allowing us to study how the strength of the 1D confinement influences  $g_m^*$ . The bow-tie (BT) device (Fig. 1a) has a conformal top-gate with a length of  $\sim 60 \mu\text{m}$  along the transport direction. The polyimide (PI) device (Fig. 1b) has a  $80 \times 80 \mu\text{m}$  top-gate separated from

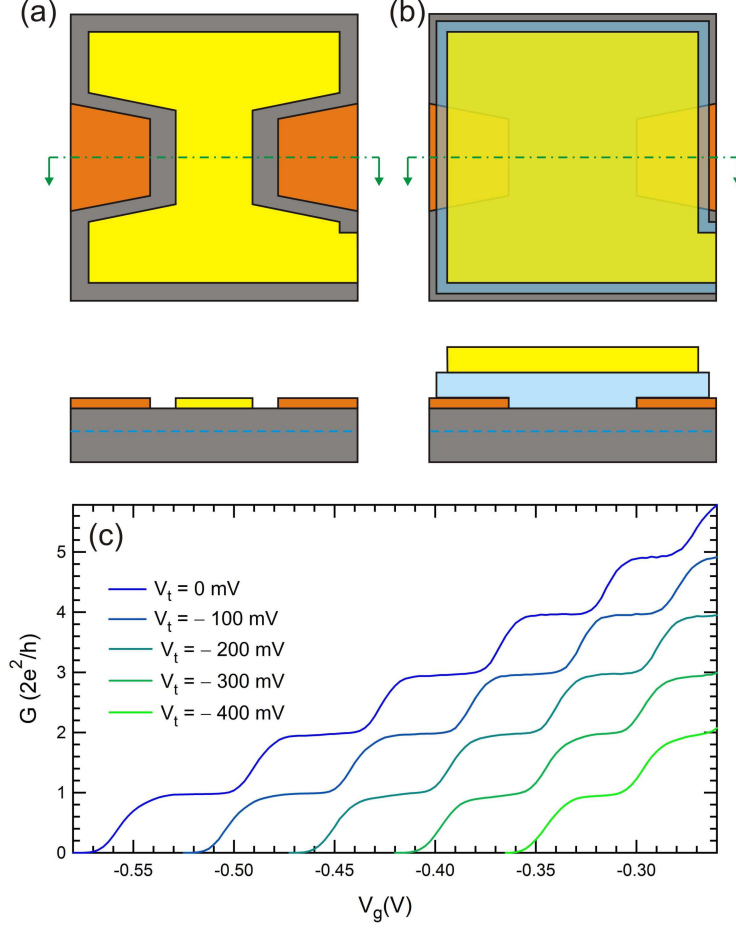


Figure 1: Top- and side-view schematics of (a) the bow-tie (BT) and (b) the polyimide (PI) devices. The side-views are sections along the green dot-dashed line. The 2DEG (blue dashed line) is located 90 nm beneath the heterostructure surface (grey). In both architectures the QPC gates (orange) define a 300 nm long, 500 nm wide constriction. The top-gate (yellow) controls the 2DEG density  $n$ , and is insulated by a 140 nm thick polyimide layer (light blue) in the PI device. Gate/insulator structures are drawn to scale. PI was measured on two separate cool-downs with the QPC gates trained whilst the top-gate was held at  $V_t = 0$  and  $+375$  mV, referred to as PI-0 and PI-375, respectively, to enable  $g_m^*$  measurements for different  $n$  ranges. (c) ac conductance  $G$  versus QPC gate voltage  $V_g$  for five different  $V_t$  settings from PI-0. For  $V_g > -0.25$  V,  $G$  rises sharply due to incomplete gate definition, limiting the density range over which  $g_m^*$  can be obtained for each 1D subband  $m$ .

the QPC gates by a 140 nm polyimide layer. The PI device was measured in two separate cool-downs, each with different top-gate ‘training’ to give a slightly different  $n$  versus  $V_t$  characteristic (see Supplementary Fig. 1). Data is presented for training at  $V_t = 0$  and  $+375$  mV, referred to as PI-0 and PI-375 hereafter, providing three separate ‘samples’ from the two device architectures. A plot of  $n$  versus  $V_t$  for each sample appears in Supplementary Fig. 2. The heterostructure used for both devices (Cambridge W0191) features a 90 nm deep 2DEG, separated from the modulation doping layer by a 40 nm undoped AlGaAs spacer. The 2DEG has a mobility of  $2.7 \times 10^6$  cm<sup>2</sup>/Vs at an ungated density of  $1.8 \times 10^{11}$  cm<sup>-2</sup> and temperature of 4 K. Further device details appear in the Supplementary Information. The devices were measured in a dilution refrigerator equipped with a 15 T superconducting solenoid and a piezoelectric rotator<sup>33</sup> for rotating the sample relative to the applied magnetic field  $B$  without the device temperature exceeding 200 mK. The density  $n$  was measured with  $B$  perpendicular to the 2DEG plane using a Fourier analysis of the Shubnikov-de Haas oscillations. Measurements of  $g_m^*$  were obtained with  $B$  oriented in-plane and along the QPC axis. To demonstrate device operation, Fig. 1c shows the ac conductance  $G$  versus  $V_g$  for five different  $V_t$  spanning the density range  $1.07 - 1.71 \times 10^{11}$  cm<sup>-2</sup> for PI-0. Conductance quantization is evident at each  $V_t$ , with pinch-off (i.e.,  $G = 0$ ) occurring for smaller  $V_g$  at more negative  $V_t$ , which reduces the Fermi energy  $E_F = \pi \hbar^2 n / m^*$  of the 2DEG reservoirs adjacent to the QPC. In each case,  $G$  rises sharply for  $V_g > -0.25$  V due to loss of electrostatic depletion under the QPC gates. This limits the number of quantized conductance plateaus observable for each  $V_t$ , and the accessible density range over which  $g_m^*$  can be obtained for a given 1D subband  $m$ .

We extract  $g_m^*$  using the method developed by Patel *et al*<sup>15</sup> to enable direct comparison with the literature.<sup>10,15,18,19</sup> Two measurements are required to extract  $g_m^*$  at each  $n$ : The first is source-drain bias spectroscopy; Fig. 2a shows a color-map of the ac transconductance  $dG/dV_g$  against source-drain bias  $V_{sd}$  ( $x$ -axis) and  $V_g$  ( $y$ -axis). The blue dotted vertical line in Fig. 2a corresponds to the left-most (blue) trace in Fig. 1c. The bright regions indicate high transconductance and correspond to the risers between plateaus, which occur when a 1D subband crosses the source/drain chemical potential  $\mu = E_F$ . With increasing  $V_{sd}$  (i.e., moving right in Fig. 2a) the source and

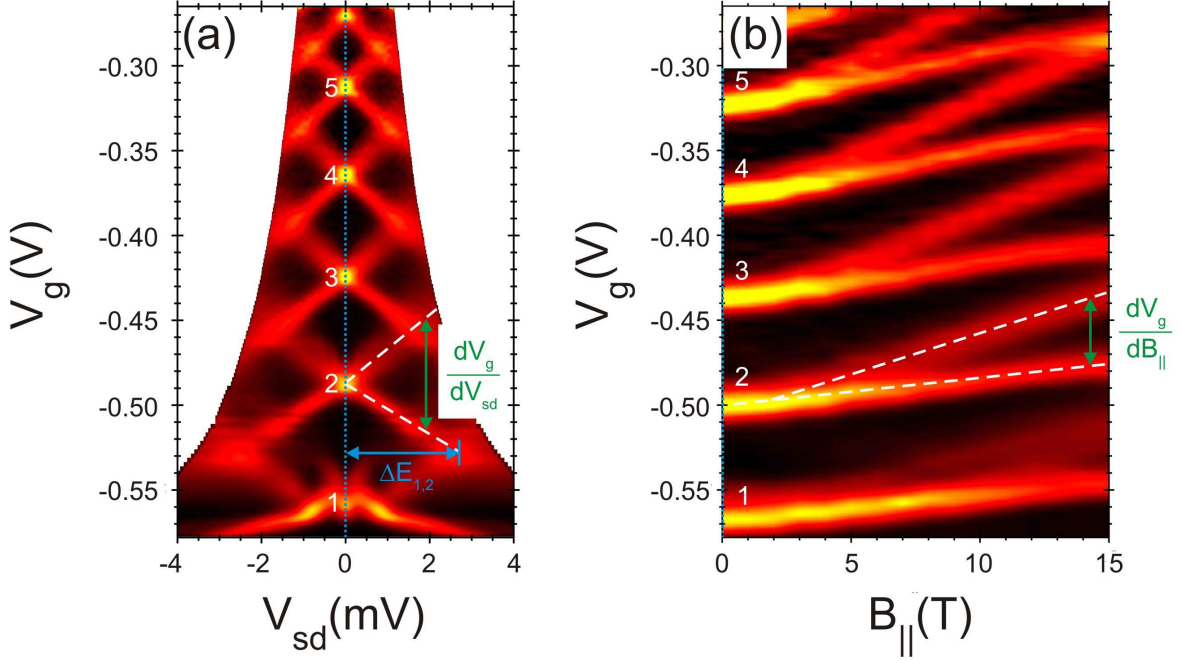


Figure 2: ac transconductance  $dG/dV_g$  vs (a)  $V_g$  (y-axis) and source-drain bias  $V_{sd}$  (x-axis) and (b)  $V_g$  (y-axis) and in-plane magnetic field  $B_{||}$  (x-axis) for PI-0 with  $V_t = 0$  V, corresponding to the left-most (blue) trace in Fig. 1c. High transconductance (risers in  $G$  between plateaus) appear bright and indicate that a given 1D subband has crossed the chemical potential  $\mu$ . The respective 1D subband indices  $m$  are superimposed in both panels. The data in (a) allows us to measure the lowest 1D subband spacing  $\Delta E_{1,2}$  and the bias-splitting rate  $dV_g/dV_{sd}$  and (b) the Zeeman splitting  $\Delta E_z$  in units of  $V_g$ . We combine the latter two measurements to obtain the  $g_m^*$  values in Fig. 3, with  $\Delta E_{1,2}$  used to characterize the confining potential in Fig. 4. The data in (a) has been symmetrized about  $V_{sd} = 0$  to remove an asymmetric background artifact arising from instrumental issues in the measurement.<sup>34</sup>

drain chemical potentials separate in energy  $\mu_s - \mu_d = eV_{sd}$  producing a bifurcation of the  $V_{sd} = 0$  transconductance maxima (white dashed lines). The rising/falling bright line corresponds to a given 1D subband coinciding with  $\mu_d$  and  $\mu_s$ , respectively. The 1D subband spacing  $\Delta E_{1,2}$  is obtained as  $eV_{sd}$  at the crossing point between the lowest rising line and the second lowest falling line (blue arrow in Fig. 2a). This provides an important measure of the ‘strength’ of the transverse confinement at the center of the QPC; however, as we discuss later, it only provides partial information about the overall confinement potential landscape of the QPC. The second measurement is the Zeeman splitting of the 1D subbands; Fig. 2b shows a color-map of  $dG/dV_g$  against in-plane magnetic field  $B_{\parallel}$  (x-axis) and  $V_g$  (y-axis). The blue dotted line corresponds to the left-most (blue) trace in Fig. 1c. Each 1D subband splits with increasing  $B_{\parallel}$  (white dashed lines); however, this does not directly yield the Zeeman splitting  $\Delta E_z$  because the y-axis has units of voltage not energy. To extract the Zeeman splitting, the splitting rates in Figs. 2a and b are combined, viz:

$$\Delta E_z = e \left[ \frac{dV_g}{dV_{sd}} \right]^{-1} \times \frac{dV_g}{dB_{\parallel}} = e \frac{dV_{sd}}{dB_{\parallel}} \quad (1)$$

giving the  $g$ -factor as  $g^* = \Delta E_z / \mu_B B_{\parallel}$ , where  $\mu_B$  is the Bohr magneton. The two terms  $\frac{dV_g}{dV_{sd}}$  and  $\frac{dV_g}{dB_{\parallel}}$  are obtained at the same  $V_g$ , making the confinement potential the same for both contributions to  $E_z$ , and hence  $g_m^*$ . Further details of the analysis appear in the Supplementary Information.

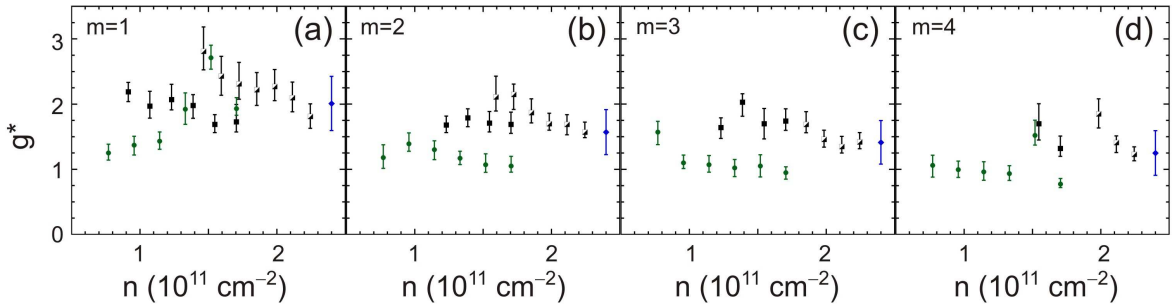


Figure 3: Plots of (a)  $g_1^*$ , (b)  $g_2^*$ , (c)  $g_3^*$  and (d)  $g_4^*$  versus 2DEG density  $n$ . The black filled squares, black half-filled squares and green circles correspond to data from PI-0, PI-375 and BT, respectively. The blue circles/error bars show the mean and standard deviation for the set of data points in each of the four panels.

We now examine how  $g_m^*$  evolves with density  $n$  for the lowest four 1D subbands, with Fig. 3a-d presenting  $g_1^*$ ,  $g_2^*$ ,  $g_3^*$  and  $g_4^*$  versus  $n$  for PI-0, PI-375 and BT. At each density  $g_m^*$  is obtained from an individually measured pair of source-drain bias and field plots similar to those in Fig. 2. The blue circle and error bar in each panel of Fig. 3 represents the mean and standard deviation for the full set of data presented in that panel; comparing these for panels a-d,  $g_m^*$  clearly increases with decreasing  $m$  on average (see also Supplementary Fig. 3), consistent with previous studies.<sup>10,15,18,19</sup> The density-dependence of  $g_m^*$  is complex and evolves with  $m$ . We start first at  $m \geq 2$ . Considering each individual device on its own for a moment, in each panel (b-d) we see that  $g_m^*$  mostly increases with decreasing  $n$ , as one would expect for exchange interactions.<sup>16</sup> However, considering the full three device data-set in each panel (b-d) there is no clear trend with density. At  $m = 1$  a distinct difference in the density dependencies for the PI and BT devices emerges (Fig. 3a): as  $n$  is reduced we observe increasing  $g_1^*$  for both PI samples but decreasing  $g_1^*$  for BT. Note also the lack of overlap in the individual  $g_1^*$  versus  $n$  behavior for PI-0 and PI-375 in the common density range  $1.5 - 1.7 \times 10^{11} \text{ cm}^{-2}$ . The findings above clearly point to a relationship between  $g^*$  and  $n$  that depends also on other parameters. It is worth noting that there is evidence for disorder effects in BT, as discussed further below, which are more prevalent than for PI-0/PI-375. One possibility that we cannot rule out at this stage is that the inherent disorder potential may also have an effect in  $g^*(n)$ . That said, given the identical heterostructure and QPC gate pattern for PI-0, PI-375 and BT, a natural expectation is that the difference is due to the top-gate; hence the logical next step is to consider the influence of the QPC confinement potential.

Precise knowledge of QPC confinement potential is difficult, it not only depends on gate bias, but also on the heterostructure doping profile and the self-consistent redistribution of charge in the 2DEG.<sup>35-37</sup> The QPC is most commonly treated as a saddle-point potential,<sup>38</sup> and while more sophisticated self-consistent models yield a flat bottomed parabola for the transverse potential,<sup>36</sup> a simple parabola is usually sufficient, particularly in the small  $m$  limit.<sup>30,39,40</sup> In a 1D parabolic well, the energy level spacing is directly tied to the curvature; hence the 1D subband spacing  $\Delta E_{m,m+1}$  is commonly used as a metric for the 1D confinement strength in QPCs.<sup>13,21,30,41-43</sup> Figure 4 shows



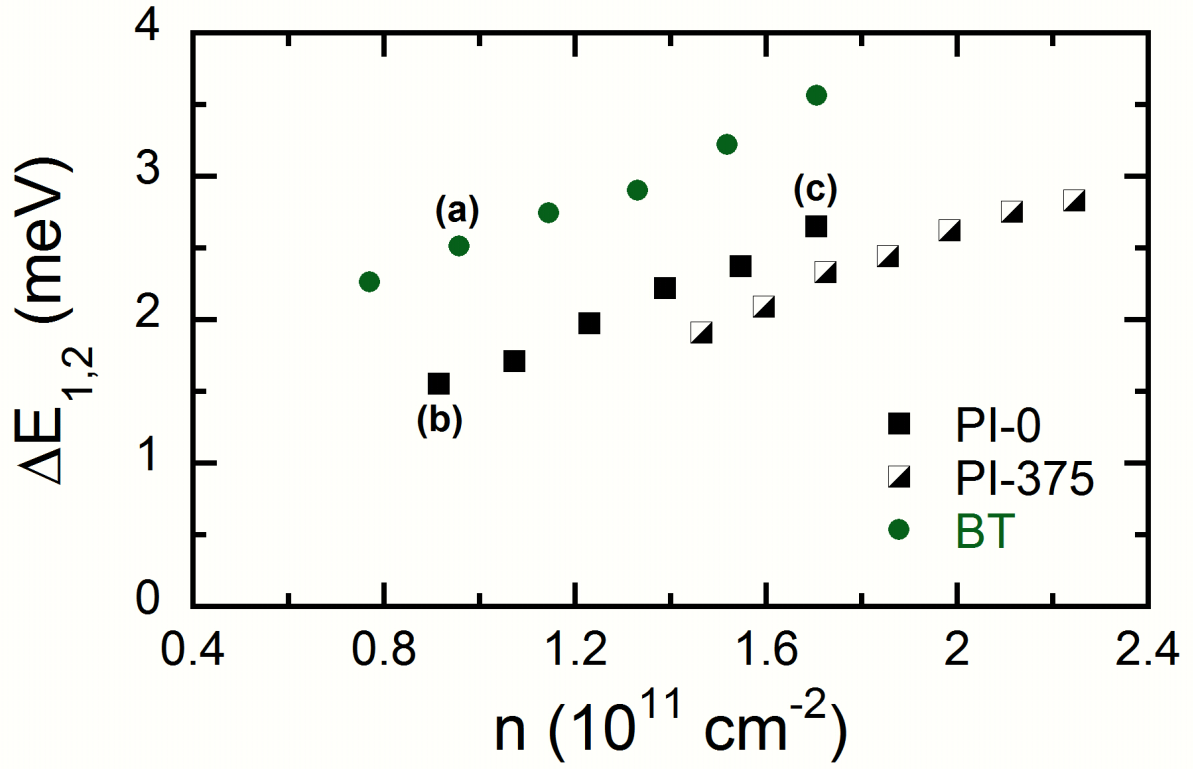


Figure 4: Plot of the lowest 1D subband spacing  $\Delta E_{1,2}$  vs density  $n$  for PI-0, PI-375 and BT. The letters (a-c) indicate the points corresponding to the data presented in Fig. 7.

the measured  $\Delta E_{1,2}$  versus  $n$  for all three samples; we focus solely on  $\Delta E_{1,2}$  due to our interest in  $g_1^*$  regarding both spintronic applications and the 0.7 anomaly. In each case  $\Delta E_{1,2}$  decreases as  $n$  is reduced, indicating a softening 1D confinement potential, consistent with earlier studies using similar device architectures.<sup>13,30</sup>

Comparing Figs. 3a and 4, an interesting but complex connection between  $g_1^*$ ,  $n$  and  $\Delta E_{1,2}$  emerges. Considering PI-0 and PI-375 alone first; their  $\Delta E_{1,2}$  versus  $n$  trends almost overlap and differ by at most 16% in the common density range  $n = 1.4 - 1.8 \times 10^{11} \text{ cm}^{-2}$ , indicating a similar 1D confinement strength. Despite this,  $g_1^*$  differs markedly ( $\sim 1.8$  for PI-0 and  $\sim 2.5$  for PI-375). Turning to PI-0 and BT over the wider density range  $n = 0.8 - 1.8 \times 10^{11} \text{ cm}^{-2}$ , the different top-gate implementation results in a  $\Delta E_{1,2}$  that is consistently  $\sim 160\%$  larger for BT than PI-0, indicating a harder, more square-well like confinement potential for BT. Yet, as Fig. 3a shows, not only can  $g_1^*$  differ markedly between PI-0 and BT at a given density, but in the former we observe increasing  $g_1^*$  and the latter decreasing  $g_1^*$  with decreasing  $n$ . Finally, at  $n = 1.7 \times 10^{11} \text{ cm}^{-2}$  where data exists for all three samples, we find  $g_1^*(\text{PI-375}) > g_1^*(\text{BT}) > g_1^*(\text{PI-0})$  whereas  $\Delta E_{1,2}(\text{BT}) \gg \Delta E_{1,2}(\text{PI-0}) \sim \Delta E_{1,2}(\text{PI-375})$ . Hence while Koop *et al*<sup>21</sup> suggest a clear and direct correlation between  $g^*$  and  $\Delta E_{1,2}$ , our data suggests the connection is much more subtle. The subband spacing  $\Delta E_{1,2}$  is only sensitive to the transverse quasi-parabolic 1D potential at the center of the QPC. As such,  $\Delta E_{1,2}$  is a limited metric of the overall shape of the QPC potential landscape, which depends on length, width, density<sup>36,44</sup> and realistically, the inherent disorder potential.<sup>45</sup> Our data suggests that  $g_1^*$  is heavily dependent on the overall QPC potential, presumably via its influence on exchange interactions within the QPC. Spin density functional theory (SDFT) calculations also point to exchange effects being very sensitive to the precise geometry of the QPC as the device approaches pinch-off.<sup>35,46,47</sup> The reduced variability in  $g^*$  with increasing  $m \geq 2$  may be due to improved screening arising from the higher electron density within the QPC (even with fixed  $n$ ).

Considering the applied implications first, when using a QPC as a spin injector/detector, one commonly applies a magnetic field to break the 1D subband degeneracy, and operates the QPC at  $G < 0.5G_0$  so that transmission is dominated by the  $1 \downarrow$  subband.<sup>3,4</sup> This makes maximizing

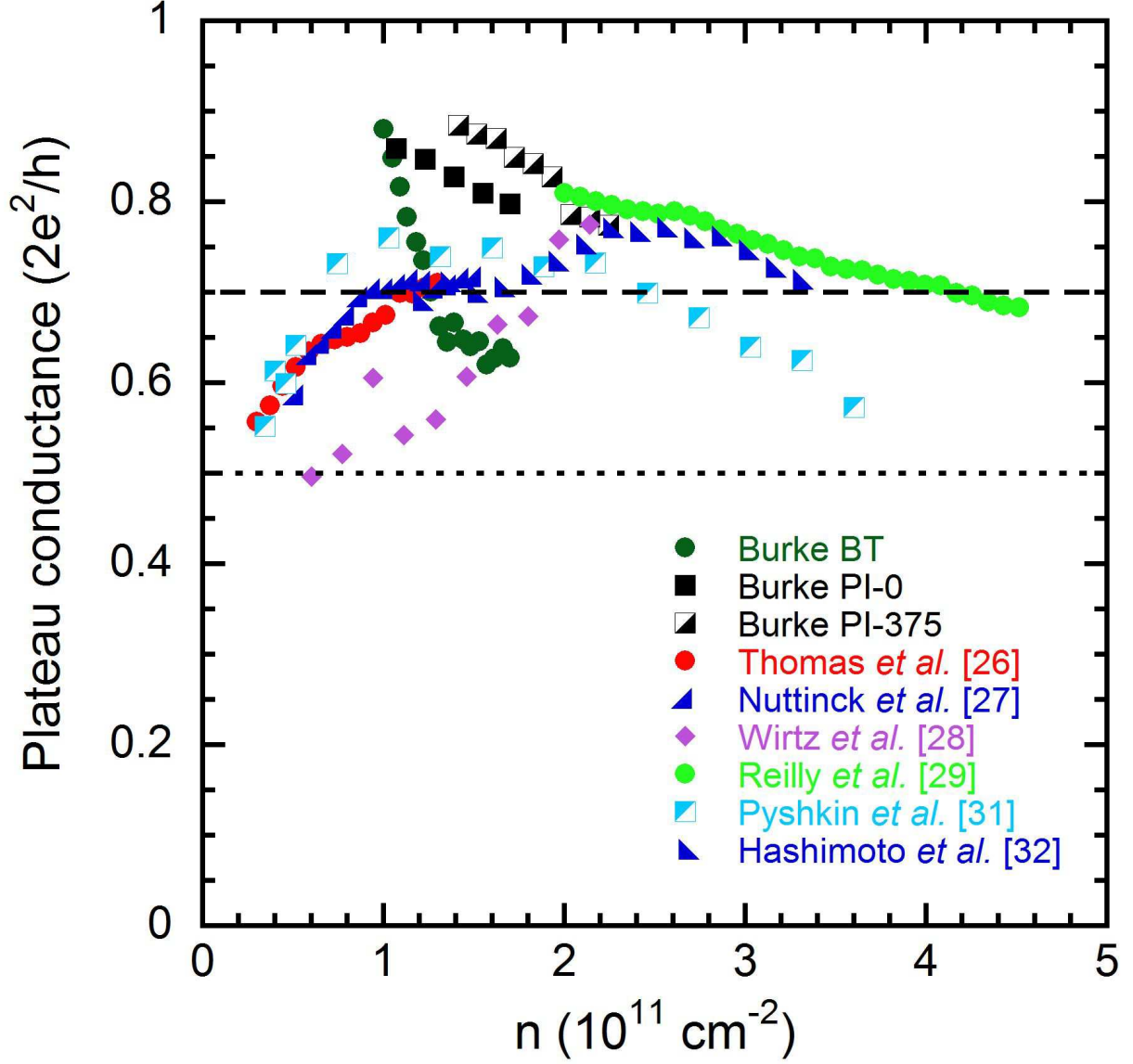


Figure 5: The precise conductance  $G$  of the 0.7 anomaly vs density  $n$  for Refs.<sup>26–29,31,32</sup> and our data from PI-0, PI-375 and BT in Fig. 6. The devices in Refs.<sup>26,29</sup> have a midline gate similar to BT (solid circles) and in Ref.<sup>31</sup> has a polyimide-insulated top-gate similar to PI (half filled squares). No simple link between the location/evolution of the 0.7 plateau and  $n$  is evident suggesting the 0.7 anomaly is heavily dependent on how the QPC is defined.

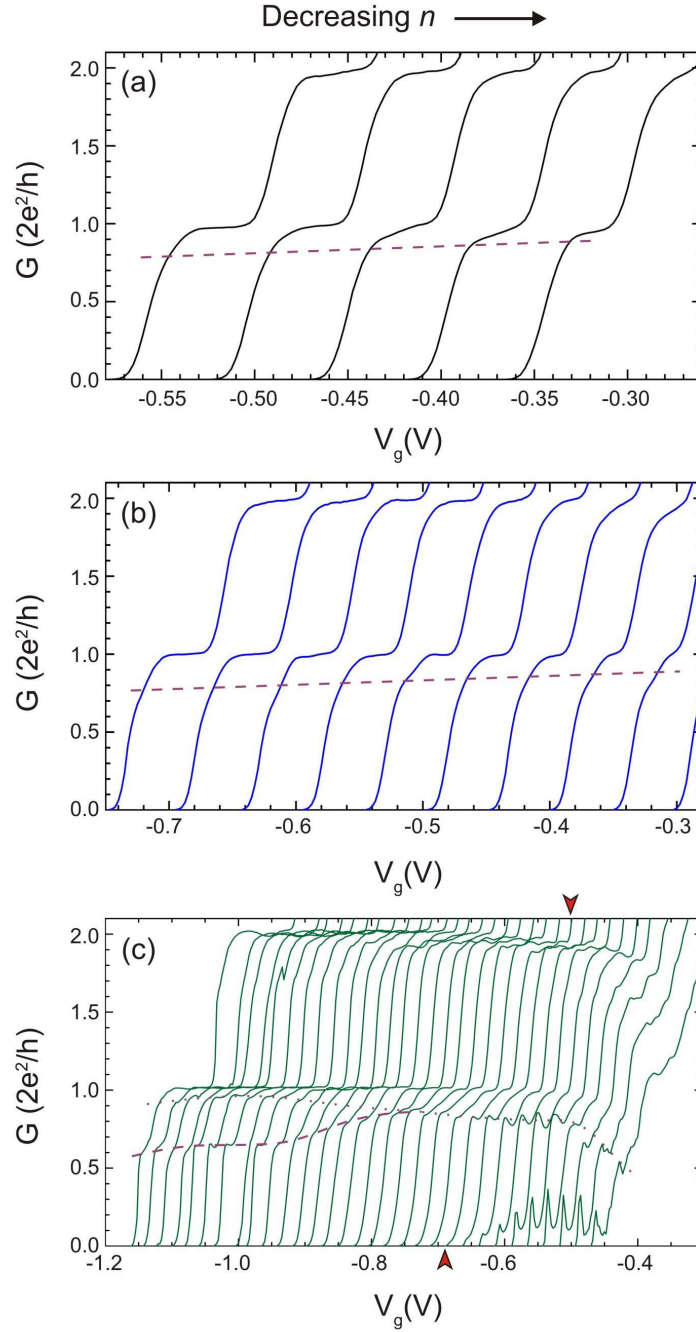


Figure 6: Conductance  $G$  versus QPC gate voltage  $V_g$  as top-gate voltage  $V_t$  is changed for (a) PI-0, (b) PI-375 and (c) BT. The  $V_t$  ranges and increments are (a) 0 (left) to  $-400$  mV (right) in steps of 100 mV, (b)  $+375$  (left) to  $-375$  mV (right) in steps of 75 mV, and (c) 0 (left) to  $-210$  mV (right) in steps of 7 mV. The purple dashed lines are guides to the eye highlighting the evolution of anomalous plateau-like structures at  $G < G_0$  with density  $n$ . The red arrows at top/bottom of (c) indicate the right-most trace from which  $g_m^*$  data is extracted.

$g_1^*$  of prime importance in reducing the magnetic field required for operation. As Fig. 3a shows, we can achieve  $g_1^*$  as large as 2.8 approaching the high values obtained in InGaAs QPCs,<sup>18</sup> and exceeding the 0.75 – 1.5 typically reported for GaAs QPCs with the field applied in the plane of the 2DEG.<sup>6,10,15,21</sup> We note that  $g^* \sim 4$  was recently reported for a GaAs QPC with the field oriented perpendicular to the 2DEG by Rössler *et al.*<sup>22</sup> Although substantially higher  $g^*$  values can be obtained in QPCs with the field perpendicular to the 2DEG,<sup>19</sup> due to the strong confinement in the heterostructure growth direction<sup>48</sup> and exchange, this comes with associated problems of cyclotron curvature, and at higher fields  $B > 1 - 2$  T, Landau quantization. These can be problematic for spintronic applications, such that in-plane fields are more commonly used; here the tight confinement of the 2DEG allows fields exceeding 10 T to be applied before cyclotron issues arise, which more than compensates for the lower  $g^*$  obtained for in-plane fields. An additional benefit of using an in-plane field to break the spin-degeneracy is that an independently variable and smaller perpendicular field component can be used to ‘steer’ a ballistic electron beam into a spin-polarized collector QPC.<sup>4,49</sup> The trends in Fig. 3a are also important, because in addition to  $g_1^*$  values as high as 2.8 we see values as low as 1.25. Hence the key to achieving and maintaining high  $g_1^*$  in QPCs is very careful management of the QPC’s confinement potential and local electrostatic environment (e.g., 2DEG density).

The evolution of  $g_1^*$  and  $\Delta E_{1,2}$  with  $n$  in Figs. 3a and 4 also provides an opportunity to address the conflict in the literature regarding the density dependence of the 0.7 anomaly. Briefly reviewing the various observations: the 0.7 plateau was reported to gradually fall towards  $0.5G_0$  with *decreasing*  $n$  in three devices: a modulation-doped midline-gated QPC<sup>26</sup> (similar to BT), a modulation-doped back-gated QPC<sup>27</sup> and a modulation-doped QPC where  $n$  was changed using illumination/hydrostatic pressure.<sup>28</sup> In contrast, the *opposite* dependence (i.e., 0.7 falls to  $0.5G_0$  with increasing  $n$ ) is observed in two other devices: an undoped QPC with a positively biased bow-tie top-gate<sup>29</sup> and a modulation-doped QPC with a mid-line gate.<sup>30</sup> Finally, a 0.7 plateau that fell towards  $0.5G_0$  with *both* increasing and decreasing  $n$  was reported for an undoped QPC with a polyimide-insulated top-gate,<sup>31</sup> and a 0.7 plateau that is strong at low and high  $n$  and which

weakens whilst rising to  $0.8G_0$  at intermediate  $n$  was reported for a modulation-doped back-gated QPC.<sup>32</sup> A summary of these results is presented in Fig. 5,<sup>1</sup> where we plot the  $G$  at which the 0.7 plateau appears against density  $n$  for the data in Refs.,<sup>26–29,31,32</sup> along with our data from Fig. 6. There is no straightforward link between the location/evolution of the 0.7 anomaly and density in Fig. 5, instead the behavior appears highly device-dependent. The QPC confinement potential is also the crux of this problem, as we now show.

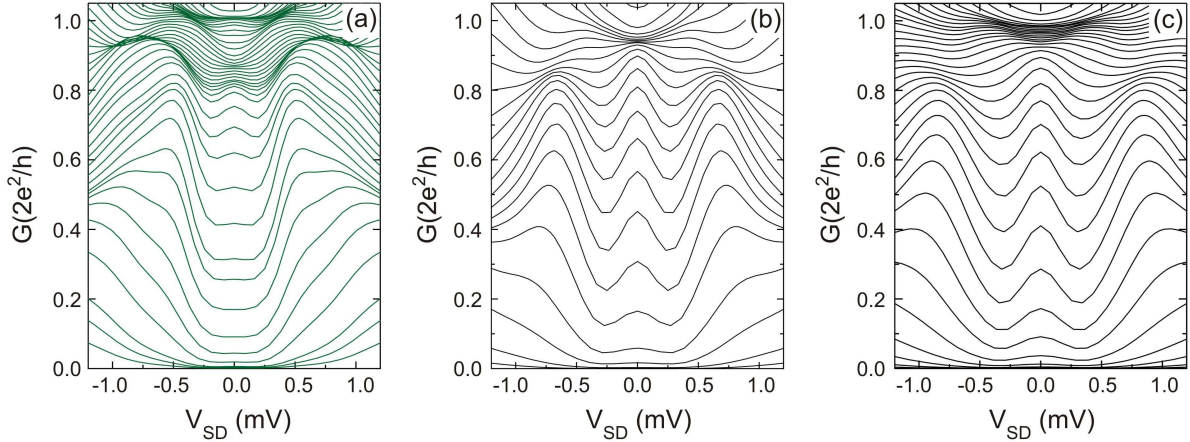


Figure 7: Differential conductance  $G'(V_{sd})$  vs source-drain bias  $V_{sd}$  for a range of  $V_g$  for (a) BT at  $V_t = -120$  mV, (b) PI-0 at  $V_t = -500$  mV and (c) 0 mV. In each case  $T < 100$  mK and  $B = 0$ , with (a)  $n = 0.95 \times 10^{11} \text{ cm}^{-2}$  and  $\Delta E_{1,2} = 2.52$  meV (b)  $n = 0.92 \times 10^{11} \text{ cm}^{-2}$  and  $\Delta E_{1,2} = 1.56$  meV, and (c)  $n = 1.70 \times 10^{11} \text{ cm}^{-2}$  and  $\Delta E_{1,2} = 2.66$  meV. The width and amplitude of the zero-bias peak (ZBP) is relatively constant with  $n$  for PI-0 and PI-375. ZBP suppression is a common feature for all  $n$  in BT. The data in each panel has been symmetrized about  $V_{sd} = 0$  to remove an asymmetric background artifact arising from instrumental issues in the measurement.<sup>34</sup>

Figure 6a-c shows  $g$  versus  $V_g$  as a function of  $V_t$  for PI-0, PI-375 and BT, respectively. The dashed purple lines highlight the evolution of the 0.7 anomaly with  $n$ . Before considering the experimental data itself, we briefly digress to consider some predictions based on the density-dependent spin-gap model introduced by Reilly *et al*,<sup>24,25</sup> since these will be vital to the discussion. The one free parameter in this model, the opening rate  $\gamma = d\Delta E_{\uparrow\downarrow}/dV_g$  of the spin-gap  $\Delta E_{\uparrow\downarrow}$  with QPC gate bias  $V_g$ , is suggested to be linked to the potential mismatch between the 1D channel and 2D reservoirs.<sup>24,25</sup> This mismatch is essentially a mode-matching effect,<sup>50,51</sup> and should be

<sup>1</sup>Results by Lee *et al*<sup>30</sup> are omitted from Fig. 5 as we are unable to precisely determine  $n$  values for this data.

dependent on the 1D confinement strength, i.e.,  $\Delta E_{1,2}$ .<sup>37,52,53</sup> Considering Fig. 3(b) of Ref.,<sup>25</sup> the prediction is that for increasing  $\gamma$  the 0.7 anomaly will move lower in  $G$  and become more pronounced. If we take the simplest assumption  $\gamma \propto \Delta E_{1,2}$ ,<sup>25</sup> two behaviors are expected given the  $\Delta E_{1,2}$  data in Fig. 4: a) the 0.7 anomaly should be weak and at higher  $G$  for PI-0 and PI-375 and be more pronounced and at lower  $G$  in BT, and b) in each case the 0.7 anomaly should weaken and tend to rise in  $G$  with decreasing  $n$ .

Considering the experimental data now; for both PI-0 and PI-375 we observe a weak inflection at relatively high  $G < G_0$  (Fig. 6(a/b)). This inflection moves to higher  $G$  with decreasing  $n$  in both cases, consistent with the corresponding reduction in  $\Delta E_{1,2}$  in Fig. 4. Because the plateau appears as a weak inflection, its weakening with decreasing  $n$  is unfortunately difficult to distinguish. However, we note that a similar rise in conductance of the 0.7 anomaly is observed with reduced  $\Delta E_{1,2}$  by Liang *et al* (see Fig. 2 of Ref.<sup>43</sup>), and here the associated weakening of the 0.7 plateau is more visible. It is also unclear whether the rise in the 0.7 feature with decreasing  $n$  is linear; a careful look at Fig. 6(b) suggests it may not be (see also Fig. 6(c)). This would mean that the assumption  $\gamma \propto \Delta E_{1,2}$  may only be approximate to the true functional relationship between  $\gamma$  and  $\Delta E_{1,2}$ . For the BT device, the 0.7 anomaly starts as a clear plateau at  $G \sim 0.6G_0$  in the high  $n$  limit. The plateau rises in conductance and weakens with decreasing  $n$ , ultimately merging in the low  $n$  limit with an additional anomalous feature dropping down from higher  $G$  with decreasing  $n$ , as highlighted by the dotted purple line. The observation of an additional plateau above the 0.7 anomaly is relatively common<sup>26,30,54,55</sup> as are small ‘bumps’ on the 0.7 anomaly at higher density.<sup>24,30</sup> The appearance of this structure in BT rather than PI is not unexpected – higher  $\Delta E_{1,2}$  is associated with a more sharply defined 1D channel, and this should enhance resonant features in the conductance, as discussed by Kirczenow.<sup>56</sup> While the BT data should be considered with care as disorder effects can modify the behaviour of the 0.7 anomaly, the 0.7 feature behavior we observe for BT is entirely consistent with expectations based on the density-dependent spin-gap model<sup>25</sup> and the behavior observed for PI-0/PI-375: The 0.7 plateau in BT is stronger and appears at a lower conductance than for the PI samples, consistent with the much higher  $\Delta E_{1,2}$  in Fig. 4. The 0.7 plateau rises

and weakens with decreasing  $n$  in each case also, following expectations based on Fig. 4 and the density-dependent spin-gap model.

One possible explanation for our observations, in particular the link between the 0.7 anomaly behavior and  $\Delta E_{1,2}$ , but also the sensitivity of  $g_1^*$ , is the formation of a quantum-dot-like localized charge state within the QPC due to the 1D-2D mismatch at the QPC openings. There is strong experimental evidence that this can occur in QPCs including observations of Kondo-like behavior,<sup>20,53,57–61</sup> Fano resonances<sup>62–64</sup> and Fabry-Pérot oscillations<sup>52</sup> on the integer conductance plateaus by other authors.<sup>2</sup> Strong exchange effects that are very sensitive to the size, shape and symmetry are a well-known feature of ultra-small quantum dots.<sup>65,66</sup> We propose that variations in the size, shape and symmetry of a quantum-dot-like localized charge state within a QPC might similarly affect the exchange interaction in QPCs, and thereby affect both the  $g$ -factor and 0.7 plateau behavior. Under this explanation, the  $g$ -factor and its sensitivity to confinement should decrease with increasing subband index. Accordingly, the magnitude of  $g^*$  decreases with increasing  $m$  in Fig. 4; however, a reduced sensitivity to confinement is not as apparent.

The mention of Kondo-like behavior above naturally leads to the question of the zero-bias peak in the differential conductance  $G'(V_{sd})$ , a feature first discussed in detail by Cronenwett *et al.*,<sup>20</sup> and commonly observed in QPCs.<sup>11</sup> The role played by Kondo physics in QPCs is heavily debated;<sup>11</sup> some suggest that Kondo physics drives the weakening of the 0.7 plateau in the low  $T$  limit,<sup>20,67</sup> others argue for the 0.7 plateau and Kondo-like physics in QPCs being separate and distinct effects.<sup>59</sup> In Fig. 7 we plot  $G'(V_{sd})$  versus  $V_{sd}$  for BT and PI-0, with  $V_t$  settings chosen to best isolate the effect of differences in  $\Delta E_{1,2}$  and  $n$  (the corresponding data points are indicated (a-c) in Fig. 4). PI-0 shows a clear zero-bias peak (ZBP) over the entire range  $0 < G < G_0$ , this ZBP behavior is consistent with most previous reports.<sup>11,20,57–59</sup> The ZBP amplitude and width for a given  $G$  are relatively independent of density (Fig. 7b/c); similar behavior is found for PI-375. In comparison, the ZBP for BT is heavily suppressed (Fig. 7a); whilst evident as a smaller amplitude peak for  $0.4G_0 < G < 0.8G_0$  it vanishes in the limits  $G \rightarrow 0$  and  $G \rightarrow G_0$ . This behavior also

---

<sup>2</sup>We also observe weak Fabry-Pérot-like structure along  $V_{sd} = 0$  in some of our source-drain bias plots (see Supplementary Fig. 4); it is much stronger in Ref.,<sup>52</sup> presumably due to the stronger 1D confinement ( $\Delta E_{1,2} \sim 5$  meV).



holds qualitatively as density is varied, but the amplitude, width and suppression vary slightly; an in-depth study will be presented elsewhere. Thermally-induced suppression of the Kondo process, and hence the ZBP, occurs as the temperature  $T$  increases relative to the Kondo temperature  $T_K$ .<sup>68</sup> In QPCs, this typically occurs for  $T > 0.5$  K.<sup>20,57,59</sup> However, in our experiment  $T$  is fixed at  $< 100$  mK; hence it must be  $T_K$  that differs between PI-0 and BT, with  $T_K^{BT} < T_K^{PI}$ . This difference in  $T_K$  is not unexpected. In quantum dots,  $T_K$  depends sensitively on the charging energy  $U$ , the bound-state energy  $\epsilon_0$  and the coupling  $\Gamma$  to the reservoirs.<sup>68</sup> These can be independently tuned in dots,<sup>68</sup> but not for a localized charge state within a QPC. Simulations predict  $\Gamma$  to be particularly sensitive to QPC potential,<sup>37</sup> but the influence of other factors such as QPC length, width, and most notably 1D-2D mismatch, i.e., 1D confinement strength  $\Delta E_{1,2}$ , are unknown. Note however that the data in Fig. 6 is consistent with a Kondo-like scenario:<sup>20,37,67</sup> for BT where the ZBP is suppressed, the 0.7 plateau is more evident and at a lower conductance than for PI, where the ZBP is stronger. The behavior in Fig. 7 cannot be tied directly to  $\Delta E_{1,2}$  or  $n$  alone; we suggest that it instead depends on the precise nature of the QPC confinement potential. The change in the ZBP we observe may indicate a change in the coupling of a single localized state to the reservoirs, or potentially to the emergence, loss, or interaction of multiple localized states within the QPC as  $G$  is driven from  $G_0$  to 0.<sup>35,69</sup>

In conclusion, we have studied the dependence of the 1D Landé  $g$ -factor  $g^*$  on density in QPCs with two different top-gate architectures. We obtain  $g^*$  values for the lowest 1D subband of up to 2.8, approaching the high values obtained in InGaAs/InP QPCs,<sup>18</sup> and significantly exceeding previously reported values for the in-plane  $g$ -factor of AlGaAs/GaAs QPCs.<sup>6,10,15,20,21</sup> Careful management of the QPC's confinement potential appears key to obtaining high  $g_1^*$ . This has important implications for using QPCs in spintronic applications. The appearance of the 0.7 plateau is strongly linked to 1D confinement potential, explaining the conflicting density dependencies reported in the literature.<sup>17,24–32</sup> In particular, the 0.7 anomaly behavior in our devices is consistent with predictions made using the density-dependent spin-gap model<sup>24,25</sup> with the one free parameter taken as directly proportional to the lowest 1D subband spacing  $\Delta E_{1,2}$ .

**Supporting Information.** Extended details of methods used, device characterization data and additional supporting data. This material is available free of charge via the Internet at <http://pubs.acs.org>.

**Corresponding author.** \*E-mail: [adam.micolich@nanoelectronics.physics.unsw.edu.au](mailto:adam.micolich@nanoelectronics.physics.unsw.edu.au)

## Acknowledgement

This work was funded by the Australian Research Council (ARC) through the Discovery Projects Scheme. APM acknowledges an ARC Future Fellowship (FT0990285). ARH acknowledges an ARC Professorial Fellowship. IF and DAR acknowledge financial support from the EPSRC. We thank T.P. Martin, U. Zülicke, D.J. Reilly and Y. Meir for helpful discussions.

## References

- (1) Awschalom, D.D.; Flatté, M.E. *Nature Physics* **2007**, *3*, 153-159.
- (2) Awschalom, D.D.; Samarth, N. *Physics* **2009**, *2*, 50-54.
- (3) Potok, R.M.; Folk, J.A.; Marcus, C.M.; Umansky, V. *Phys. Rev. Lett.* **2002**, *89*, 266602.
- (4) Folk, J.A.; Potok, R.M.; Marcus, C.M.; Umansky, V. *Science* **2003**, *299*, 679-682.
- (5) Debray, P.; Rahman, S.M.S.; Wan, J.; Newrock, R.S.; Cahay, M.; Ngo, A.T.; Ulloa, S.E.; Herbert, S.T.; Muhammad, M.; Johnson, M. *Nature Nanotech.* **2009**, *4*, 759-764.
- (6) Frolov, S.M.; Venkatesan, A.; Yu, W.; Folk, J.A.; Wegscheider, W. *Phys. Rev. Lett.* **2009**, *102*, 116802.
- (7) Frolov, S.M.; Lüscher, S.; Yu, W.; Ren, Y.; Folk, J.A.; Wegscheider, W. *Nature* **2009**, *458*, 868-871.
- (8) van Wees, B.J.; van Houten, H.; Beenakker, C.W.J.; Williamson, J.G.; Kouwenhoven, L.P.; van der Marel, D.; Foxon, C.T. *Phys. Rev. Lett.* **1988**, *60*, 848-850.

- (9) Wharam, D.A.; Thornton, T.J.; Newbury, R.; Pepper, M.; Ahmed, H.; Frost, J.E.F.; Hasko, D.G.; Peacock, D.C.; Ritchie, D.A.; Jones, G.A.C. *J. Phys. C* **1988**, *21*, L209-L214.
- (10) Thomas, K.J.; Nicholls, J.T.; Simmons, M.Y.; Pepper, M.; Mace, D.R.; Ritchie, D.A. *Phys. Rev. Lett.* **1996**, *77*, 135-138.
- (11) Micolich, A.P. *J. Phys.: Condens. Matter* **2011**, *23*, 443201.
- (12) Auslaender, O.M.; Steinberg, H.; Yacoby, A.; Tserkovnyak, Y.; Halperin, B.I.; Baldwin, K.W.; Pfeiffer, L.N.; West, K.W. *Science* **2005**, *308*, 88-92.
- (13) Hew, W.K.; Thomas, K.J.; Pepper, M.; Farrer, I.; Anderson, D.; Jones, G.A.C.; Ritchie, D.A. *Phys. Rev. Lett.* **2008**, *101*, 036801; *Phys. Rev. Lett.* **2009**, *102*, 056804.
- (14) Deshpande, V.V.; Bockrath, M.; Glazman, L.I.; Yacoby, A. *Nature* **2010**, *464*, 209-215.
- (15) Patel, N.K.; Nicholls, J.T.; Martín-Moreno, L.; Pepper, M.; Frost, J.E.F.; Ritchie, D.A.; Jones, G.A.C. *Phys. Rev. B* **1991**, *44*, 10973-10975.
- (16) Janak, J.F. *Phys. Rev.* **1969**, *178*, 1416-1418.
- (17) Thomas, K.J.; Nicholls, J.T.; Appleyard, N.J.; Simmons, M.Y.; Pepper, M.; Mace, D.R.; Tribe, W.R.; Ritchie, D.A. *Phys. Rev. B* **1998**, *58*, 4846-4852.
- (18) Martin, T.P.; Szorkovszky, A.; Micolich, A.P.; Hamilton, A.R.; Marlow, C.A.; Linke, H.; Taylor, R.P.; Samuelson, L. *Appl. Phys. Lett.* **2008**, *93*, 012105.
- (19) Martin, T.P.; Szorkovszky, A.; Micolich, A.P.; Hamilton, A.R.; Marlow, C.A.; Taylor, R.P.; Linke, H.; Xu, H.Q. *Phys. Rev. B* **2010**, *81*, 041303.
- (20) Cronenwett, S.M.; Lynch, H.J.; Goldhaber-Gordon, D.; Kouwenhoven, L.P.; Marcus, C.M.; Hirose, K.; Wingreen, N.S.; Umansky, V. *Phys. Rev. Lett.* **2002**, *88*, 226805.
- (21) Koop, E.J.; Lerescu, A.I.; Liu, J.; van Wees, B.J.; Reuter, D.; Wieck, A.D.; van der Wal, C.H. *J. Supercond. Nov. Magn.* **2007**, *20*, 433-441.

- (22) Rössler, C.; Baer, S.; de Wiljes, E.; Ardelt, P.-L.; Ihn, T.; Ensslin, K.; Reichl, C.; Wegscheider, W. *New J. Phys.* **2011**, *13*, 113006.
- (23) Schäpers, T.; Guzenko, V.A.; Hardtdegen, H. *Appl. Phys. Lett.* **2007**, *90*, 122107.
- (24) Reilly, D.J.; Buehler, T.M.; O'Brien, J.L.; Hamilton, A.R.; Dzurak, A.S.; Clark, R.G.; Kane, B.E.; Pfeiffer, L.N.; West, K.W. *Phys. Rev. Lett.* **2002**, *89*, 246801.
- (25) Reilly, D.J. *Phys. Rev. B* **2005**, *72*, 033309.
- (26) Thomas, K.J.; Nicholls, J.T.; Pepper, M.; Tribe, W.R.; Simmons, M.Y.; Ritchie, D.A. *Phys. Rev. B* **2000**, *61*, 13365-13368.
- (27) Nuttinck, S.; Hashimoto, K.; Miyashita, S.; Saku, T.; Yamamoto, Y.; Hirayama, Y. *Jpn. J. Appl. Phys.* **2000**, *39*, L655-L657.
- (28) Wirtz, R.; Newbury, R.; Nicholls, J.T.; Tribe, W.R.; Simmons, M.Y.; Pepper, M. *Phys. Rev. B* **2002**, *65*, 233316.
- (29) Reilly, D.J.; Facer, G.R.; Dzurak, A.S.; Kane, B.E.; Clark, R.G.; Stiles, P.J.; Hamilton, A.R., O'Brien, J.L.; Lumpkin, N.E.; Pfeiffer, L.N.; West, K.W. *Phys. Rev. B* **2001**, *63*, 121311.
- (30) Lee, H.-M.; Muraki, K.; Chang, E.Y.; Hirayama, Y. *J. Appl. Phys.* **2006**, *100*, 043701.
- (31) Pyshkin, K.S.; Ford, C.J.B.; Harrell, R.H.; Pepper, M.; Linfield, E.H.; Ritchie, D.A. *Phys. Rev. B* **2000**, *62*, 15842-15850.
- (32) Hashimoto, K.; Miyashita, S.; Saku, T.; Hirayama, Y. *Jpn. J. Appl. Phys.* **2001**, *40*, 3000-3002.
- (33) Yeoh, L.A.; Srinivasan, A.; Martin, T.P.; Klochan, O.; Micolich, A.P.; Hamilton, A.R. *Rev. Sci. Instrum.* **2010**, *81*, 113905.

- (34) Kristensen, A.; Bruus, H.; Hansen, A.E.; Jensen, J.B.; Lindelof, P.E.; Marckmann, C.J.; Nygård, J.; Sørensen, C.B.; Beuscher, F.; Forchel, A.; Michel, M. *Phys. Rev. B* **2000**, *62*, 10950.
- (35) Rejec, T.; Meir, Y. *Nature* **2006**, *442*, 900-903.
- (36) Laux, S.E.; Frank, D.J.; Stern, F. *Surf. Sci.* **1988**, *196*, 101-106.
- (37) Hirose, K.; Meir, Y.; Wingreen, N.S. *Phys. Rev. Lett.* **2003**, *90*, 026804.
- (38) Büttiker, M. *Phys. Rev. B* **1990**, *41*, 7906-7909.
- (39) Weisz, J.F.; Berggren, K.-F. *Phys. Rev. B* **1989**, *40*, 1325-1327.
- (40) Kardynał, B.; Barnes, C.H.W.; Linfield, E.H.; Ritchie, D.A.; Nicholls, J.T.; Brown, K.M.; Jones, G.A.C.; Pepper, M. *Phys. Rev. B* **1997**, *55*, 1966-1969.
- (41) Thomas, K.J.; Simmons, M.Y.; Nicholls, J.T.; Mace, D.R.; Pepper, M.; Ritchie, D.A. *Appl. Phys. Lett.* **1995**, *67*, 109-111.
- (42) Kristensen, A.; Bo Jensen, J.; Zaffalon, M.; Sørensen, C.B.; Reimann, S.M.; Lindelof, P.E.; Michel, M.; Forchel, A. *J. Appl. Phys.* **1998**, *83*, 607-609.
- (43) Liang, C.-T.; Simmons, M.Y.; Smith, C.G.; Kim, G.H.; Ritchie, D.A.; Pepper, M. *Phys. Rev. B* **1999**, *60*, 10687-10690.
- (44) Iqbal, M.J.; de Jong, J.P.; Reuter, D.; Wieck, A.D.; van der Wal, C.H. arXiv:1207.1331.
- (45) Nixon, J.A.; Davies, J.H.; Baranger, H.U. *Phys. Rev. B* **1991**, *43*, 12638-12641.
- (46) Akis, R.; Ferry, D.K. *J. Phys.: Condens. Matter* **2008**, *20*, 164201.
- (47) Berggren, K.-F.; Yakimenko, I.I. *J. Phys.: Condens. Matter* **2008**, *20*, 164203.
- (48) Kowalski, B.; Omling, P.; Meyer, B.K.; Hofmann, D.M.; Wetzel, C.; Härle, V.; Scholz, F.; Sobkowicz, P. *Phys. Rev. B* **1994**, *49*, 14786-14789.

- (49) Rokhinson, L.P.; Larkina, V.; Lyanda-Geller, Y.B.; Pfeiffer, L.N.; West, K.W. *Phys. Rev. Lett.* **2004**, *93*, 146601.
- (50) Glazman, L.I.; Lesovik, G.B.; Khmel'nitskii, D.E.; Shekter, R.I. *JETP Lett.* **1988**, *48*, 238-241.
- (51) Szafer, A.; Stone, A.D. *Phys. Rev. Lett.* **1989**, *62*, 300-303.
- (52) Lindelof, P.E.; Aagesen, M. *J. Phys.: Condens. Matter* **2008**, *20*, 164207.
- (53) Wu, P.M.; Li, P.; Zhang, H.; Chang, A.M.; *Phys. Rev. B* **2012**, *85*, 085305.
- (54) Crook, R.; Prance, J.; Thomas, K.J.; Chorley, S.J.; Farrer, I.; Ritchie, D.A.; Pepper, M.; Smith, C.G. *Science* **2006**, *312*, 1359-1362.
- (55) Thomas, K.; Nicholls, J.T.; Simmons, M.Y.; Pepper, M.; Mace, D.R.; Ritchie, D.A. *Phil. Mag. B* **1998**, *77*, 1213-1218.
- (56) Kirczenow, G. *Phys. Rev. B* **1989**, *39*, 10452-10455.
- (57) Komijani, Y.; Csontos, M.; Shorubalko, I.; Ihn, T.; Ensslin, K.; Meir, Y.; Reuter, D.; Wieck, A.D. *Europhys. Lett.* **2010**, *91*, 67010.
- (58) Klochan, O.; Micolich, A.P.; Hamilton, A.R.; Trunov, K.; Reuter, D.; Wieck, A.D. *Phys. Rev. Lett.* **2011**, *107*, 076805.
- (59) Sfigakis, F.; Ford, C.J.B.; Pepper, M.; Kataoka, M.; Ritchie, D.A.; Simmons, M.Y. *Phys. Rev. Lett.* **2008**, *100*, 026807.
- (60) Chen, T.-M.; Graham, A.C.; Pepper, M.; Farrer, I.; Ritchie, D.A. *Phys. Rev. B* **2009**, *79*, 153303.
- (61) Sarkozy, S.; Sfigakis, F.; Das Gupta, K.; Farrer, I.; Ritchie, D.A.; Jones, G.A.C.; Pepper, M.; *Phys. Rev. B* **2009**, *79*, 161307.

- (62) Yoon, Y.; Mourokh, L.; Morimoto, T.; Aoki, N.; Ochiai, Y.; Reno, J.L.; Bird, J.P. *Phys. Rev. Lett.* **2007**, *99*, 136805.
- (63) Yoon, Y.; Kang, M.-G.; Morimoto, T.; Mourokh, L.; Aoki, N.; Reno, J.L.; Bird, J.P.; Ochiai, Y. *Phys. Rev. B* **2009**, *79*, 121304.
- (64) Yoon, Y.; Kang, M.-G.; Morimoto, T.; Kida, M.; Aoki, N.; Reno, J.L.; Ochiai, Y.; Mourokh, L.; Fransson, J.; Bird, J.P. *Phys. Rev. X* **2012**, *2*, 021003.
- (65) Kouwenhoven, L.P.; Austing, D.G.; Tarucha, S. *Rep. Prog. Phys.* **2001**, *64*, 701-736.
- (66) Hanson, R.; Kouwenhoven, L.P.; Petta, J.R.; Tarucha, S.; Vandersypen, L.M.K. *Rev. Mod. Phys.* **2007**, *79*, 1217-1265.
- (67) Meir, Y.; Hirose, K.; Wingreen, N.S. *Phys. Rev. Lett.* **2002**, *89*, 196802.
- (68) Goldhaber-Gordon, D.; Shtrikman, H.; Mahalu, D.; Abusch-Magder, D.; Meirav, U.; Kastner, M.A.; *Nature* **1998**, *391*, 156.
- (69) Meir, Y.; Private communication.